

# Soft Matter

Accepted Manuscript



This is an *Accepted Manuscript*, which has been through the Royal Society of Chemistry peer review process and has been accepted for publication.

*Accepted Manuscripts* are published online shortly after acceptance, before technical editing, formatting and proof reading. Using this free service, authors can make their results available to the community, in citable form, before we publish the edited article. We will replace this *Accepted Manuscript* with the edited and formatted *Advance Article* as soon as it is available.

You can find more information about *Accepted Manuscripts* in the [Information for Authors](#).

Please note that technical editing may introduce minor changes to the text and/or graphics, which may alter content. The journal's standard [Terms & Conditions](#) and the [Ethical guidelines](#) still apply. In no event shall the Royal Society of Chemistry be held responsible for any errors or omissions in this *Accepted Manuscript* or any consequences arising from the use of any information it contains.



# The Chinese University of Hong Kong

*Department of Chemistry  
Shatin, N.T, Hong Kong*

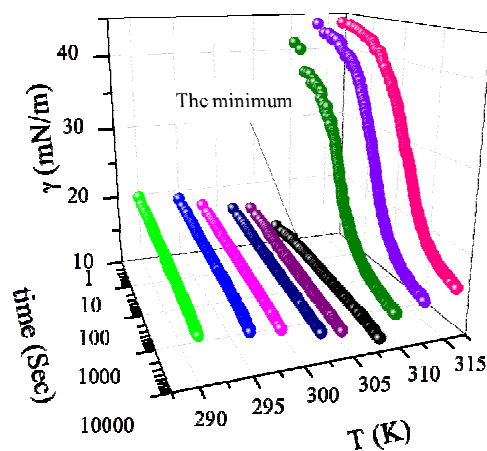
To NGAI, Ph.D.

☎ : (+852) 3943 1222

☎ : (+852) 2603 5057

## Graphical abstract:

The heptane-water interfacial tension exhibits a minimum in the presence of PNIPAM microgels, particularly in the vicinity of volume phase transition temperature (VPTT) of PNIPAM microgels. The origin of such interfacial tension minima contributes to the microgel spreading at the oil-water interface at the early states, and then governs by the microgels packing and interactions at the final static equilibrium states.



# Poly(*N*-isopropylacrylamide) Microgels at the Oil-Water Interface: Temperature Effect

Zifu Li<sup>1</sup>, Walter Richtering<sup>2\*</sup>, and To Ngai<sup>3\*</sup>

1. *Department of Chemical and Materials Engineering, University of Alberta, Edmonton T6G 2G6, AB, Canada*
2. *Institute of Physical Chemistry, RWTH Aachen University, Landoltweg 2, D-52056 Aachen, Germany*
3. *Department of Chemistry, The Chinese University of Hong Kong, Shatin, N. T., Hong Kong*

\* To whom correspondence should be addressed.

*Email:*

*tongai@cuhk.edu.hk; Tel: (852)-39431222, Fax: (852)-26035057,*

*richtering@rwth-aachen.de; Tel: +49(0)2418094760, Fax: +49(0)2418092327.*

**Abstract**

Understanding interfacial properties of soft poly(*N*-isopropylacrylamide) (PNIPAM) microgels covered oil-water interface is essential for engineering stimuli-responsive emulsions stabilized by soft microgel particles. This paper presents a systematic study on the interfacial properties of the PNIPAM microgels laden heptane-water interface as a function of temperature. We measured the interfacial tensions as well as dilatational rheology properties of microgels laden heptane-water interface using a pendant drop tensiometer. From fresh droplet experiments, anomalous interfacial tension minima of the microgels covered oil-water interface are observed in the vicinity of volume phase transition temperature (VPTT) of PNIPAM microgels. Such interfacial tension minima are observable regardless of microgels aggregates. Both dynamic and static parameters contributed to the observed interfacial tension minima around VPTT. PNIPAM microgel deformability dynamically dominated the microgel spreading at the heptane-water interface at the early states, while PNIPAM microgels packing and interactions dominated the final static equilibrium states. Combined the interfacial tensions and the dilatational rheology properties, we propose microgels would approach three distinctive states at temperatures below, around, and above VPTT at the heptane-water interface. Single droplet experiments further demonstrate that there exists an irreversible transition among these three states. The revealed results in this paper deepen our understanding of soft, porous, and deformable microgels' behaviors at the oil-water interface, and have important implications for engineering microgels as stimuli-responsive emulsion stabilizers.

## Introduction

Emulsions with controllable stability are highly desirable in many industrial processes, as breaking normal emulsions is difficult and costly, and also produces large amount of unwanted waste.<sup>1</sup> Low molecular weight switchable surfactants have received tremendous attention, but the recycling is difficult, greatly limiting their wide applications.<sup>1</sup> Stabilizers based on larger colloidal particles are thus more promising.<sup>2-6</sup> Among them, poly(*N*-isopropylacrylamide) (PNIPAM) based microgels, which exhibit a well-known volume phase transition temperature (VPTT) at around 32°C,<sup>7-11</sup> have received significant attention in the past few years. They are surface-active, arrange around droplets, and make highly stable emulsions. More importantly, the responsiveness of microgels offer the possibility to get stimuli-sensitive emulsions for which the particle interactions at the interface may be tuned *in situ* and consequently the emulsion can be broken on demand by changing the external parameters, such as the temperature and the pH value.<sup>12, 13</sup> These peculiar properties brought some interesting applications, for example, in biocatalysis.<sup>2-6, 14-30</sup> Nevertheless, the origin of emulsion responsiveness was obscure, mainly because the mechanism of emulsion stabilization and destabilization by microgels were not understood and thus needed further investigations.<sup>31-33</sup>

By incorporation of ionic co-monomer, such as methacrylic acid (MAA) into PNIPAM microgels, one of our groups has systematically studied the effect of solution pH on PNIPAM-*co*-MAA microgel layers at the oil-water interface.<sup>3-5, 14, 27, 28, 32, 34</sup> First, it was observed that the heptane-water interfacial tension in the presence of microgels at pH 3 was lower than that at pH 9, indicating that microgels are surface-active even at the neutral state. Second, via Cryo-SEM, the heptane-water interface was found to be densely covered with microgels at pH 3 to form crystal-like structures; whereas at pH 9, loosely packed microgels layers with linkages and clusters were presented.<sup>4</sup> However, the emulsions at pH 9 were more stable than that at pH 3. To explain such counterintuitive packing-emulsion stability relationship, it was suggested that the interfacial visco-elastic properties of the microgel layers played a dominant role in determining the stability of microgel-stabilized emulsions.<sup>5</sup>

On the other hand, regarding to the effect of temperature on PNIPAM microgel layers at the oil-water interface, two different PNIPAM-based microgels systems have been investigated. Using pure PNIPAM microgels, Destribats *et al.* reported that the initially spherical microgels adopted a “fried egg-like” structure when adsorbed at the oil-water interface and that the interfacial deformation was greatly increased as the crosslink densities decreased.<sup>19</sup> Once the crosslink density or the temperature was increased, the deformability of microgels was lost, and the stabilization efficiency was considerably reduced. Therefore, the authors correlated the microgel deformability to the emulsions stability. However, it is important to note that less attention has been paid to the temperature triggered interfacial properties of microgel covered interfaces.<sup>35</sup> After copolymerizing dimethylaminoethylmethacrylate (DMAEMA) to

PNIPAM microgels and used them to stabilize the emulsions, Monteux *et al.* observed an interfacial tension minimum around the VPTT of PNIPAM microgels at the *n*-dodecane-water interface.<sup>35</sup> They also noticed that the emulsion droplets started coalescence around the same temperature range. They argued that the formation of more compact microgel layers or an increase in the number of adsorbed microgel at the interface led to the decrease of interfacial tensions when the temperature was first slightly increased. However, as the temperature was further increased above VPTT, microgels could form loosely packed heterogeneous hydrophobic aggregates/precipitates at the *n*-dodecane-water interface due to the poor bulk solvent conditions. These aggregates/precipitates eventually resulted in the formation of unprotected contacts (holes) between droplets. The combination of these two effects (increased number of adsorbed microgel at temperature below VPTT and aggregates/precipitates above VPTT) likely induced the breaking of the water film to separate droplets and hence emulsion droplets started coalescence and ultimately phase separation. To support their argument, they showed the formation of microgel tablets at the *n*-dodecane-water interface when the temperature was risen to 45 °C. Besides, they mentioned that such microgel tablets were also observable at the surface of aqueous microgel solutions.<sup>35</sup> Note that using pure PNIPAM microgels (without using DMAEMA comonomers in the synthesis), they also observed the interfacial tension minimum around VPTT. Therefore, whether the existence of the incorporated DMAEMA is necessity or not, as well as the origin of the observed interfacial tension minimum, needs to be further explored.

In this paper, we present a systematic study on the interfacial properties of the heptane-water interface covered with pure PNIPAM microgels using a pendant drop tensiometer.<sup>21</sup> Specifically, we measured the interfacial tensions and dilatational rheology properties as a function of temperature by both fresh and single droplet approaches.<sup>36-39</sup> Anomalous interfacial tension minima of the microgel covered heptane-water interface in the vicinity of VPTT were always found, with fresh droplets method. Our results suggested that the formation of these interfacial tension minima could be ascribed to the deformability and the packing as well as the interactions of these microgels at the oil-water interface. Based on these results, we propose that microgels would approach three distinctive states at temperatures below, around, and above VPTT, respectively. Single droplet experiments further reveal that there exists an irreversible transition among these three states with microgels laden at the heptane-water interface. The revealed results have important implications for engineering microgels as stimuli-responsive emulsion stabilizers.

## Materials and Methods

**Materials:** *N*-isopropylacrylamide (NIPAM, Sigma) was recrystallized from a toluene/*n*-hexane mixture. *N,N'*-methylenebis-(acrylamide) (BA or BIS, Fluka), potassium persulfate (KPS, Merck), and heptane

(Sigma) were used as received without any purification. The fluorescent dye methacryloxyethylthiocarbamoyl rhodamine B (MRB, Polysciences, Inc.) was used as received. Deionized water was used in all experiments.

**Microgels Preparations:** To simplify our study, pure PNIPAM microgels (no functional comonomers were added in the synthesis) with crosslink density of 3.2% BA were prepared and employed for the pendant drop experiments.<sup>7, 8, 10, 21</sup> Typically, NIPAM (4.50 g), BA (0.15 g), and the fluorescent dye, MRB 0.005 g, were dissolved into 500 mL of deionized water in a 1000 mL three-neck reactor fitted with nitrogen bubbling inlet and outlet, and a reflux condenser and stirred with a mechanical stir. After stirring the solution for 40 min at 70 °C under nitrogen bubbling, the polymerization was initiated by adding of potassium persulfate ( $K_2S_2O_8$ , KPS) dissolved in 10 mL of deionized water. The reaction was kept at 70 °C for 7 hours and then cooled to room temperature. After that, the dispersion was passed through glass wool to get rid of large aggregates and further purified by five times centrifugation at 10000 g.

**Microgels Characterizations:** The synthesized 3.2%BA microgels were characterized with various techniques. First, the size of the synthesized microgels was measured by laser light scattering (LLS) and one typical size distribution of the microgel sample is shown in Fig. S1. The apparatus used for LLS measurements was a modified commercial light-scattering spectrometer equipped with an ALV-5000 multi- $\tau$  digital time correlator and a He-Ne laser (output power = 22 mW at  $\lambda_0 = 632\text{nm}$ ). In dynamic laser light scattering (DLS), the intensity-intensity time correlation function  $G^{(2)}(\tau)$  in the self-beating mode was measured in the scattering angle range  $17.5^\circ - 150^\circ$ . The Laplace inversion of  $G^{(2)}(\tau)$  can lead to a line-width distribution  $G(I)$ , which can be further converted to a translational diffusive coefficient distribution  $G(D)$  by  $I = Dq^2$  or a hydrodynamic radius distribution  $f(R_h)$  by use of the Stokes-Einstein equation,  $R_h = k_B T / (6\pi\eta D)$ , where  $\eta$ ,  $k_B$ , and  $T$  are the solvent viscosity, the Boltzmann constant, and the absolute temperature, respectively.<sup>40</sup> The electrophoretic mobility  $\mu_e$  of the 3.2%BA microgels was measured using a Zeta-potential analyzer (Zeta-Plus, Brookhaven). Six measurements were done to obtain the average result,  $\mu_e$  was  $-1.21 \pm 0.01 \times 10^{-8} \text{ m}^2 \text{ V}^{-1} \text{ s}^{-1}$  at 10 mM NaCl and 298 K. Consider that microgels diameter around 500 nm and that the Debye length 10 nm at 10 mM NaCl solution, the thin double layer can be applied and the correspondence Zeta-potential is  $-15.53 \pm 1.47 \text{ mV}$ .<sup>41</sup> This low value indicates that these pure PNIPAM microgels are slightly negatively charged, originating from the residual sulfate groups by initiator KPS. We also measured that the microgels electrophoretic mobility  $\mu_e$  in 1 mM NaCl was  $-0.21 \pm 0.04 \times 10^{-8} \text{ m}^2 \text{ V}^{-1} \text{ s}^{-1}$  at 298 K and  $-2.05 \pm 0.61 \times 10^{-8} \text{ m}^2 \text{ V}^{-1} \text{ s}^{-1}$  at 314 K, respectively. Transmission Electron Microscopy (TEM) was also applied to characterize the microgels. For TEM observation, one drop of the diluted microgels ( $10^{-5} \text{ g/mL}$ ) was first placed on the copper grid, dried at room temperature for 24 h and then imaged with FEI CM120 at 120 kV. Typical TEM result was shown in Fig. S2, the dried microgels had average diameter around 300 nm, and they

were very uniform.

**Pendant Drop Tensiometer for Studying Microgels at the Oil-Water Interface:** The principle of the pendant drop tensiometer is detailed elsewhere,<sup>42-45</sup> and can also be found in Drop Shape Analysis (DSA) for DSA 100, User manual V1.9-03. The key for DSA is that the instrument record one single droplet image, which is then fitted with theoretical curves to obtain the best fitting interfacial tension. DSA is carried out on a DSA100 (Krüss GmbH, Hamburg, Germany) equipped with a pendant drop module. The image analysis is done with the help of the Drop Shape Analysis program (Version 1.01) supplied by the manufacturer. Droplet volume  $V$ , droplet interfacial area  $A$ , and interfacial tension  $\gamma$  can be calculated, usually with the highest rate possible (approximately 1 reading/ 1 s). The choice of oil has a large influence on the microgel-stabilized emulsions.<sup>12, 18, 27</sup> Here, the heptane-water interface is chosen as a model system due to the following two advantages: first, most of the previous reports focused on the heptane-water emulsions system so that the obtained results can be compared with those previous measurements; second, heptane-water interface is rather simple in comparison with other oil-water interface, such as octanol-water interface. The interfacial tension of pure heptane-water interface is about  $51 \times 10^{-3} \text{N/m}$ , while for octanol-water, the value is about  $8.5 \times 10^{-3} \text{N/m}$ . Moreover, heptane has lower solubility ( $3 \times 10^{-6} \text{g/g}$ ) in water compared with octanol ( $2.3 \times 10^{-3} \text{g/g}$ ). Therefore, all the investigation of microgel interfacial behaviors would be carried out at the heptane-water interface in the presence of microgels. The density difference between water and heptane is 0.314 g/ml. For dilute microgels solutions, the density has been increased only a little, thus the density difference between water and heptane is still applied. Fig. S3 shows one typically created pendant droplet for the investigation of the PNIPAM microgels interfacial adsorption behaviors at the heptane-water interface at 294 K. After formation, the shape of this droplet evolves as PNIPAM microgels adsorb to the interface. Normally, the droplets were left for two hours to reach the equilibrium. Afterwards, the microgels covered heptane-water interfacial dilatation rheology experiments were further carried out with an ODM-Module for the DSA100 (Krüss GmbH, Hamburg, Germany). The volume and the area of the droplet as well were varied by applying a voltage to the piezo-driven membrane. The voltage was varied with a fixed frequency at 0.1 Hz and the deformation amplitude (range from 10 to 30% referred to the maximum voltage) for each measurement. A video of the oscillating drop was analyzed with the help of the software package supplied by the manufacture (Drop shape analyzer). To guaranty a stable temperature, the cuvette was placed in a chamber and the temperature was controlled with an external cryostat. The temperature can be controlled within  $\pm 0.1 \text{ K}$ .

## Results and discussion

Fresh microgel droplets were created at various temperatures and hung in heptane; pendant drop tensiometer recorded the dynamic interfacial tensions (Fig. S3).<sup>21, 44, 46-49</sup> Fig. 1 shows the temperature dependence of the heptane-water dynamic interfacial tensions when the interface is gradually covered by microgels (microgel concentration was fixed at  $5 \times 10^{-3}$  g/mL). At the same time, the dynamic interfacial tension,  $\gamma_t$ , decreases when the temperature increases from 286 to 308 K, but further increase of temperature leads to increased  $\gamma_t$ . It seems that  $\gamma_t$  has a minimum value at 308.1 K compared with  $\gamma_t$  at other temperatures. Fig. 2 shows the corresponding temperature dependence of the meso-equilibrium interfacial tension ( $\gamma_m$ ) at the heptane-water interface after 6000 seconds. Similar to Monteux's report,<sup>35</sup>  $\gamma_m$  decreases with the increasing temperature until a minimum value is reached at 308.1 K, close to VPTT of the PNIPAM microgels.  $\gamma_m$  increases when the temperature is further increased above VPTT.

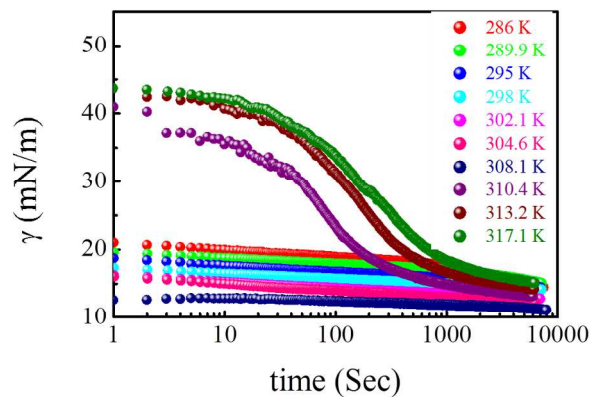


**Fig. 1** The dynamic interfacial tension  $\gamma_t$  of the heptane-water interface in the presence of PNIPAM microgels at various temperatures.

To have a clear view of the  $\gamma_t$  as a function of temperature and time, three-dimensional (3D) plot related to the  $\gamma_t$ , time, and temperature was created and shown in Fig. 3. Obviously, an interfacial tension minimum is observed at 308.1 K. In our recent study,<sup>21</sup> we had correlated the heptane-water interfacial tensions with microgel adsorption behaviours via the surface pressures, and this correlation can be described in Eq. (1).<sup>47</sup>

$$\Pi_t = \gamma_p - \gamma_t = \Gamma_t RT \quad (1)$$

where  $\Gamma_t$  is the interfacial PNIPAM microgels concentration,  $\Pi_t$  is the surface pressure, and  $\gamma_p$  is the pure heptane-water interfacial tension. Thus, the observed interfacial tension minimum could reflect the differences in PNIPAM microgels dynamic adsorption behaviours at the heptane-water interface at varied

temperatures.<sup>21, 50-53</sup>

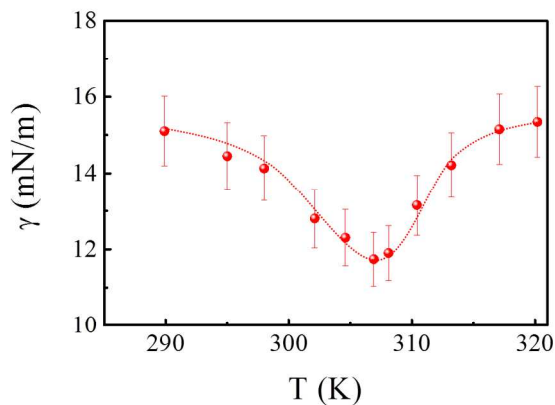


**Fig. 2** The meso-equilibrium interfacial tension,  $\gamma_m$  of the heptane-water interface in the presence of PNIPAM microgels at various temperatures.

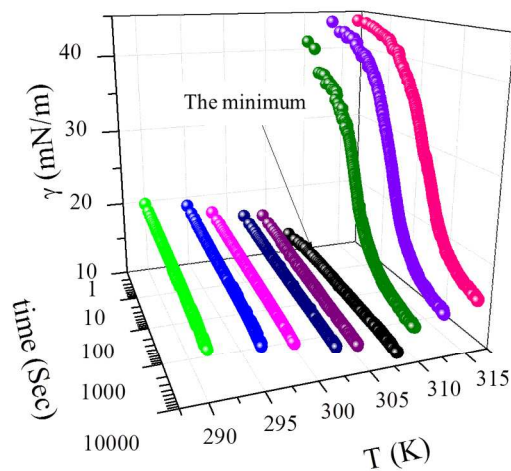


**Fig. 3.**  $\gamma_t$ -time-temperature three dimensional plots of the heptane-water interface in the presence of PNIPAM microgels. Note that a minimum can be observed at temperature around VPTT (308.1 K).

The heptane-water  $\gamma_t$  was also investigated in the presence of PNIPAM microgels dispersed in various NaCl solutions so as to test the salt effect on microgel adsorption behaviors at the heptane-water interface. To ensure that sufficient amount of microgels were in the bulk phase and exclude the effect from diffusion-determined process, all these measurements were carried out at relatively high microgel concentration (*i.e.*,  $5 \times 10^{-3} \text{ g/mL}$ ) with various NaCl concentrations.<sup>21</sup> At 298 K, the presence of NaCl

exerted little influence on microgel adsorption behavior. As shown in Fig. S4,  $\gamma_t$  collapsed into one similar curve with nearly constant  $\gamma_m$  ( $\sim 14$  mN/m) either in the presence or absence of NaCl (Fig. S5 shows  $\gamma_m$  at various salt concentrations) at 298 K. Fig. S6 shows the heptane-water  $\gamma_t$  in the presence of PNIPAM microgels dispersed in 0.5 mM NaCl at varied temperatures. Similar to microgel behavior in pure water, the minimum of  $\gamma_t$  is found at 304 K. A three-dimensional plot regarding to  $\gamma_t$ , time, and temperature clearly showed that the interfacial tension at 304 K always had a minimum (Fig. S7). Similar results were also obtained in the presence of 2.75 mM NaCl at various temperatures (Fig. S8). Different adsorption behaviours were observed by dispersing PNIPAM microgels in 10 mM NaCl solution, as shown in Fig. S9. At temperature below VPTT, the heptane-water  $\gamma_t$  had a similar behavior to that in pure water and in 0.5 or 2.75 mM NaCl solutions. The initial interfacial tensions decrease with increasing temperature and a minimum curve is observed at 305.1 K. However, distinct behaviors were obtained at temperature above VPTT. Specifically, at 307, 310.9 and 317.5 K,  $\gamma_t$  rapidly decreased and directly fell into the meso-equilibrium regime, as shown in Fig. S9. Note that at low NaCl concentrations or pure water and above VPTT,  $\gamma_t$  usually first undergoes a long induction period and then decreases gradually, as shown in Figs. 1 and S6.

As crosslinker BA reacts faster than NIPAM monomer, most of the BA might locate at the core, and thus PNIPAM microgel commonly adopted a core-corona structure.<sup>9, 10, 54, 55</sup> At temperature below VPTT, these microgels can be viewed as polymeric networks as highly crosslinked cores and less crosslinked corona with dangling chains. These PNIPAM microgels are stabilized via steric repulsion with these periphery dangling chains.<sup>9</sup> At temperature above VPTT, PNIPAM microgel is also stable. Mostly, microgel is stabilized with effective negative charges, originating from the sulphate groups of KPS initiators (see Zeta potential measurements in materials and methods).<sup>56, 57</sup> However, its stability could be easily destroyed by tuning the experimental conditions. For example, introduction of salt could significantly screen the electrostatic repulsions, leading to the microgel aggregation at high temperatures.<sup>58</sup> Fig. S10 shows that for 3.2%BA microgels, aggregation occurs at the heptane-water interface at 10 mM NaCl solution at temperature above VPTT (50 °C). Besides, we also found that these microgels aggregated at the water-air interface when they were dispersed in 10 mM NaCl solution, as shown in Fig. S11. All these aggregates (both at the heptane-water interface and water-air interface) were still found even the temperature was cooled down and after stayed at room temperature for 24 hours, indicating that the aggregation of microgels is irreversible. In other experimental conditions with lower NaCl concentrations, 3.2%BA PNIPAM microgels were always stable and did not aggregate. Therefore, the observed dynamic interfacial tension differences at 10 mM NaCl at temperature above VPTT (see Fig. S9) can be ascribed to these PNIPAM microgel aggregates. At 10 mM NaCl and at temperature above VPTT, microgels form larger aggregates. Because of these aggregates' larger size, the gravity force

cannot be neglected. Driven by the gravity force, these aggregates adsorb onto the heptane-water interface faster compared to that of individual microgel, shortening the induction and rapid fall regimes, as shown in Fig. S9. Whereas, in the cases at lower NaCl concentrations (0, 0.5, and 2.75 mM), microgels did not aggregate, and the gravity force of individual microgel can be negligible.

Though the observed differences existed when 3.2%BA PNIPAM microgels were dispersed in 10 mM NaCl solution above VPTT,  $\gamma_t$  still exhibited a minimum around VPTT, as shown in Fig. S9. To summarize, the minimum value of  $\gamma_m$  is always observed at various salt concentrations, as shown in Fig. 4. This phenomenon may not be well explained by PNIPAM microgels aggregates, which only affect the microgel adsorption dynamics at the heptane-water interface.

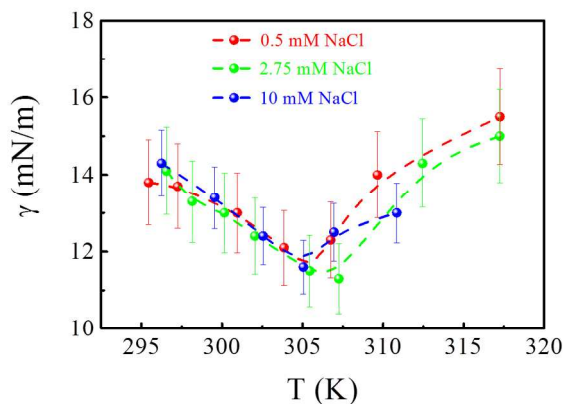


**Fig. 4** The summary of temperature dependence of  $\gamma_m$  of the heptane-water interface in the presence of various NaCl concentrations.

From the above results and discussion, the interpretations given by Monteux *et al.* for explaining the temperature dependence on interfacial tension in the presence of PNIPAM microgels may need to be re-examined. The main reason is that microgel used in their study may lose the colloidal stability in the designed experiments. The used microgels were polymerized at pH 4 with cationic initiators V50 and comonomer, DMAEMA.<sup>35</sup> The resultant microgel is expected to be stable at high temperature (above VPTT) in the polymerization conditions. After purification, residue poly-DMAEMA chains were removed, which were confirmed by the NMR results. But during the interfacial tension measurements, they changed the microgel solution pH to 9. At pH 9 and high temperature, these microgels become unstable, and then aggregate. This could be the reason why tablets were observed at the surface of microgel solutions as well as at the *n*-dodecane-water interface. However, the formation of microgel tablet cannot well explain the decrease of interfacial tension when temperature approaches VPTT. The

condition of our PNIPAM microgels dispersed in 10 mM NaCl solution is similar to their investigations at pH 9 and high temperature. Hence, the formation of microgel tablets at the *n*-dodecane-water interface cannot satisfactorily explain why the interfacial minimum is formed in the vicinity of PNIPAM microgel VPTT.

Fig. 5 shows that the size of the microgels holds constant at temperature above 310 K and that 3.2%BA microgels had a VPTT around 305 K, in good agreement with previous reports.<sup>9, 10</sup> Hence, the effective microgel volume fraction holds constant. Note that  $R_h$  of microgels decreases from 220 to around 86 nm when the temperature increases from 290 to 310 K, indicating that the effective microgel volume fraction decreases with increasing temperature.<sup>9, 10</sup> Therefore, the observed interfacial tension minimum shown in Fig. 3 cannot be attributed to the PNIPAM microgel collapse upon heating, or the decreased volume fraction of microgel.

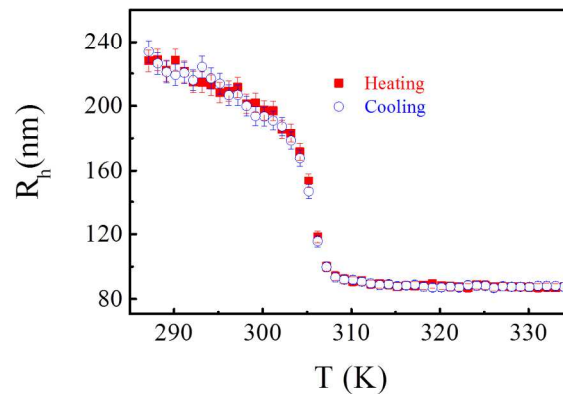


**Fig. 5.** Typical collapse and swell processes of 3.2%BA PNIPAM microgels under the heating and cooling processes in deionized water.

To account for the observed interfacial tension minima around VPTT, PNIPAM microgels adsorption dynamics should be first taken into consideration, because the interfacial tension minimum formed from the beginning and retained in the whole measuring periods, as shown in Fig. 3. In our recent study, we came to the conclusion that PNIPAM microgels adsorption onto the heptane-water interface was dominated by two steps.<sup>21</sup> Microgels first diffused from aqueous phase to the heptane-water interface, and this diffusion process was mainly governed by microgel concentration. After arrival at the heptane-water interface, microgels deformed and spread at the interface, and this dynamic spreading process was mainly dominated by microgels' deformability.<sup>21, 59, 60</sup> It is worthy pointing out that all of our measurements were carried out at a microgel concentration of  $5 \times 10^{-3}$  g/mL. We have shown that at this concentration with

temperature of 317 K, diffusion had limited influence on microgels adsorption behaviours to the heptane-water interface. Presumably, it could be related to the microgels' deformability dominated spreading process at the heptane-water interface, especially at the initial state.<sup>21, 59</sup>

Recent AFM measurements have shown that the Young's modulus ( $E$ ) of PNIPAM microgel exhibited a minimum value around VPTT. The fully collapsed single microgel ( $E = 123$  kPa) was about ten times stiffer than a fully swollen one ( $E = 13$  kPa). More importantly, a dramatic softening of the microgel was found near the transition temperature at about 310 K ( $E = 3$  kPa).<sup>61</sup> The observed smallest value of  $E$  was considered originating from the softening of microgel's bulk modulus ( $K$ ). The value of  $K$  was determined via measuring the volume deformation of the microgel as a function of osmotic pressure using dextran solutions.<sup>62</sup> Using a capillary micromechanics approach, it further showed that PNIPAM microgel's compressive modulus first decreased with increasing temperature, reached a minimum around VPTT, and then increased with increasing temperature above VPTT, exhibiting a dip in the Poisson ratio close to VPTT.<sup>63</sup> And the softening transition behaviors of PNIPAM microgels had been qualitative captured with Flory-Rehner theory, similar to PNIPAM bulk gels.<sup>64</sup>

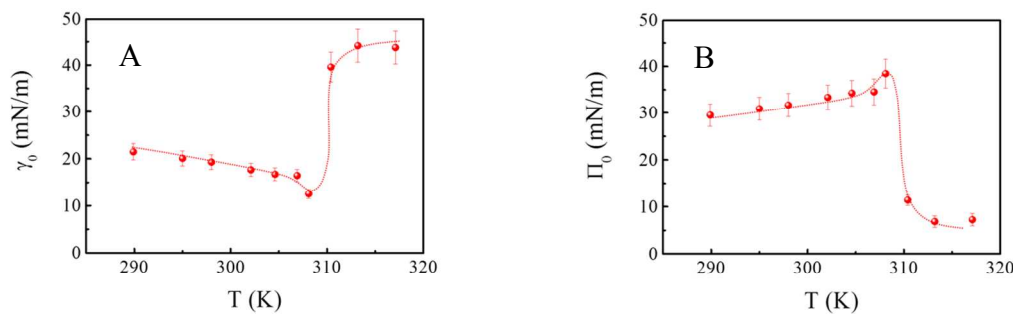


**Fig. 6.** A),  $\gamma_0$  of the heptane-water interface at various temperatures; B),  $\Pi_0$  of the heptane-water interface at various temperatures.

Fig. 6A shows that the initial heptane-water interfacial tension ( $\gamma_0$ ), in the presence of sufficient PNIPAM microgels, has a minimum around VPTT (308.1 K). Note that the data in Fig. 6 is extracted from Fig. 1. The corresponding initial surface pressure ( $\Pi_0$ ) exhibits a maximum at the same temperature (Fig. 6B). According to Eq. (1), the observed surface pressure maximum indicates that interfacial coverage by microgels reaches a maximum value around VPTT. The softening effect of microgels might provide the clue for explaining the observed interfacial tension minimum at the initial state.<sup>21, 59, 63</sup> At temperature below VPTT, due to the high deformability and typical core-corona structures with dangling chains of PNIPAM microgels, spreading can easily proceed. However, at temperature above VPTT, the collapsed microgels undergo relatively slow spreading process at the heptane-water interface so that the

interfacial tension decreases slowly at high temperatures.<sup>21, 59</sup>

The above results and discussions shed light on why an interfacial tension minimum forms at the initial state. However, the microgel deformability cannot fully explain why the minimum retains in the whole measuring periods, as shown in Fig. 3. Fig. 6A shows that at temperatures below VPTT, all the initial interfacial tensions directly decline to around 20 mN/m, indicating that the spreading of PNIPAM microgel is very fast below VPTT. According to previous Cryo-SEM results that 75% PNIPAM microgel interfacial coverage corresponds to  $\gamma = 15$  mN/m and  $\Pi = 36$  mN/m at the heptane-water interface, all these initial interfacial coverage exceeds 56%.<sup>4, 19</sup> At such high microgel interfacial coverage, extra microgels cannot freely adsorb to the densely packed interface.<sup>21, 60</sup> The initial adsorbed microgels might be forced to rearrange themselves to provide enough space for new microgel adsorption. Such processes undergo in a very slow rate, as shown in Fig. 1, and they are not only controlled by microgels deformability but also by the interactions between adsorbed microgels as well as these microgels and the novel adsorbed microgels (the packing of microgels at the interface).<sup>65-68</sup> At temperatures above VPTT, the deformability controlled spreading process proceed quite slow: at low microgel interfacial coverage, microgel can freely spread at the heptane-water interface; at high microgel interfacial coverage, similar to the case at temperatures below VPTT, the interactions between microgels would also exert large influence on new microgel adsorption to the heptane-water interface. And the interactions among microgels are different at temperatures below and above VPTT.<sup>65, 67, 68</sup>

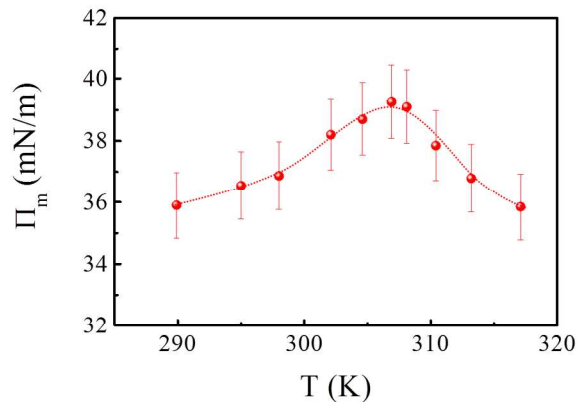


**Fig. 7.**  $\Pi_m$  of the heptane-water interface at varied temperatures.

Due to the slow rearrangement process, it would take extremely long time for these adsorption processes to approach, if they can, their static equilibrium states.<sup>21, 47</sup> After microgels adsorbed to the heptane-water interface for around 6000 seconds, all  $\gamma_t$  curves enter the meso-equilibrium regimes and

the interfacial tension minimum is still observable, as shown in Fig. 3. Fig. 7 shows the corresponding temperature dependence of meso-equilibrium surface pressures ( $\Pi_m$ ) at the heptane-water interface. According to Eq. (1), Fig. 7 is identical to Fig. 2. All surface pressures exceed 35 mN/m, indicating that all these microgels interfacial coverage surpass 72%. A surface pressure maximum is also observed. Thus, below the maximum point, one specific surface pressure would correspond to two states, above and below VPPT, respectively.

To differentiate these two states at the same surface pressure, dilatational rheology is applied for the characterization of the microgels covered interfaces. The principles of the dilatational rheology are detailed elsewhere.<sup>46, 69</sup> Fig. 8 shows the complex modulus ( $E^*$ ) of the microgels covered heptane-water interface measured at various temperatures. All these measurements were carried out at frequency 0.1 Hz, and the deformations varied from 10% to 30%. Clearly, a complex modulus ( $E^*$ ) minimum was observed at 308.1 K.

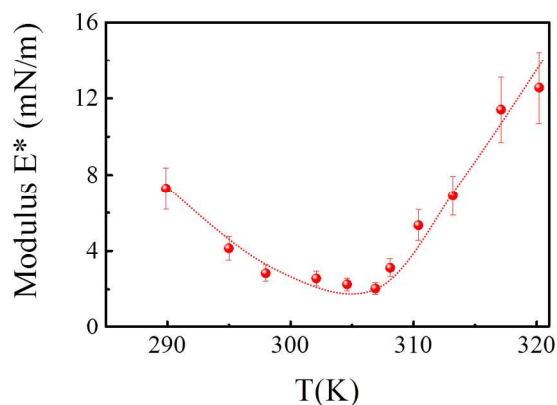


**Fig. 8.** Complex modulus ( $E^*$ ) of the PNIPAM microgels covered heptane-water interface at varied temperatures.

Complex modulus  $E^*$  is a complex parameter, and can be divided into two parts: the real (the elastic modulus  $E'$ ) and the imaginary part (the loss modulus  $E''$ ).<sup>46, 69</sup>

$$E^* = E' + iE'' \quad (2)$$

Fig. 9 shows the elastic ( $E'$ ) and loss ( $E''$ ) moduli of the microgels covered heptane-water interface at various temperatures. In the entire temperature range,  $E'$  is always larger than  $E''$ , indicating solid-like behaviours. Also  $E'$  exhibits a minimum around 308.1 K; while  $E''$  stays in a plateau at temperature below VPPT and increases slightly at temperature above VPPT.

Generally, the dilatational modulus versus surface pressure curve is plotted to obtain the surface

equation of state of the adsorbed proteins at the given interface, and it is a sensitive tool for assessing non-ideal behaviour in the adsorbed protein layer. Usually, the results with the different protein concentrations could collapse to form a master curve that is typical for that protein.<sup>70</sup> The PNIPAM microgel covered interface dilatational elastic modulus ( $E'$ ) is plotted versus surface pressure ( $\Pi$ ) and presented in Fig. 10. Elastic modulus decreases with increasing surface pressure, both at temperature above and below VPTT. More importantly, different elastic modulus values were obtained at the same surface pressure value. This clearly demonstrates that the interactions between the adsorbed microgels at the heptane-water interface are different at temperatures below and above VPTT at the same interfacial coverage.

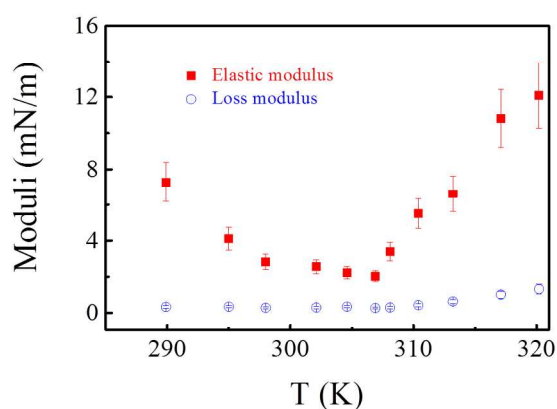


**Fig. 9.** Moduli ( $E'$ ,  $E''$ ) of PNIPAM microgels covered heptane-water interface, at varied temperatures.

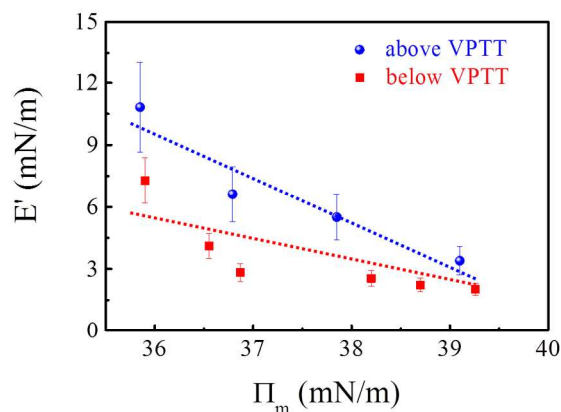


**Fig. 10.**  $E'$  as a function of  $\Pi_m$  of the heptane-water interface in the presence of PNIPAM microgels (the dotted lines were plotted for eye guiding).

Based on our observed dynamic interfacial tension minima and the interfacial dilatational rheology results at the meso-equilibrium regimes from fresh droplet experiments, we propose that PNIPAM microgels would approach to different static equilibrium states at varied temperatures due to their varied physical properties and interactions.<sup>10, 34, 56</sup> With microgels of varied physical properties at different temperatures, three typical distinct single PNIPAM microgels layer would form at the heptane-water interface, considering the size and the interactions of these microgels at varied experimental conditions, as shown in Fig. 11. Due to the steric repulsions between peripheries chains at temperature below VPTT and the electrostatic repulsions between residue sulphate groups at temperature above VPTT,<sup>56, 57</sup> these two PNIPAM microgels layers (A and C) pack sparser than that at temperature around VPTT at the heptane-water interface. Therefore, a microgels interfacial coverage maximum would form after microgels densely packed at the heptane-water interface around VPTT. Hence, the heptane-water interfacial tension would exhibit a minimum at the highest microgels interfacial coverage around VPTT. The proposed three typical distinct single microgels layers represent three typical static equilibrium states with microgels at varied temperatures at the heptane-water interface. The microgels would always adsorb to the heptane-water interface to lower the interfacial tension, but the adsorption rate would become increasing slower with increasing microgels interfacial coverage. Therefore, the experimental observed minimum might retain in an extremely long time (Fig. 3).

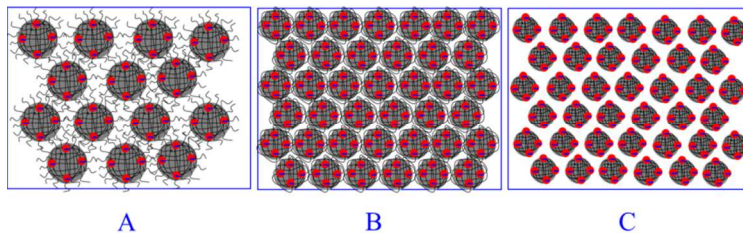


**Fig. 11.** Three proposed distinct single microgel layer at the heptane-water interface at various experimental conditions (flat in-plane interface are depicted instead of curved interface and the microgels are purposely arranged in a hexagon pattern to obtain the highest interfacial coverage): A) at temperature below VPTT; B) at temperature around VPTT; and C) at temperature above VPTT.

To have a comprehensive understanding of temperature effect on the microgels covered heptane-water interface properties, another two experiments adopting the single droplet method were carried out.<sup>36, 37, 39</sup> As shown in Fig. S12, the first single droplet was initially created at 295 K (microgel concentration was still  $5 \times 10^{-3}$  g/mL), equilibrated for two hours to let microgels fully adsorb onto the heptane-water interface and to reach the thermal equilibrium; afterwards, it was successively heated to 320 K (at a rate of 1K/min), equilibrated for one hour to reach the thermal equilibrium, and then cooled back to 295 K, the starting temperature (cooling rate 1K/min, more details on the experimental procedures are provided in

supporting information). Fig. 12 shows the change of  $\gamma$  as a function of temperature. First, with this single droplet method  $\gamma$  is around 12 mN/m at 320 K. This value is lower than the value ( $\sim 15$  mN/m) obtained from fresh droplet method, as shown in Fig. 2. This difference clearly demonstrates that different ways of preparing the droplets affect the interfacial tensions. Second, during the cooling process,  $\gamma$  returns back, though the value becomes slightly smaller than initial value. Presumably, this slight difference is originated from the hysteresis between microgels response and thermal conduction. Table 1 summarizes the moduli of this single droplet at three conditions: initial 295 K, 320 K, and back 295 K. With this single droplet method  $E$  is around 3.98 mN/m at 320 K. This value is lower than the value ( $\sim 12$  mN/m) obtained from fresh droplet method, as shown in Fig. 9. This difference reconfirms that different ways of preparing the droplets affect the properties of the microgel-laden heptane-water interface. More importantly, both the interfacial tension and moduli (complex modulus, elastic modulus, and loss modulus) can return to the initial values after this thermal circle (the heating and cooling processes).

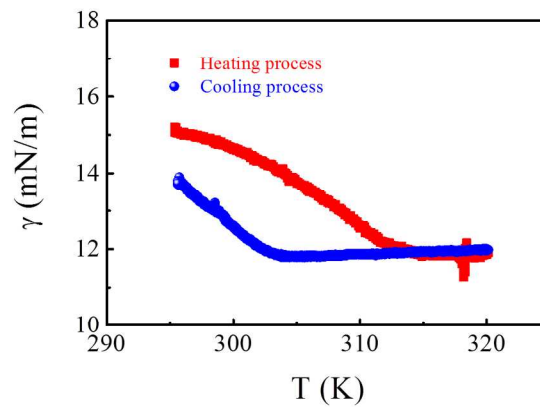


**Fig. 12.** The dynamic interfacial tension  $\gamma_t$  of single droplet, starting at 295 K, in the presence of PNIPAM microgels at various temperatures.

	Complex Modulus $E^*$ (mN/m)	Elastic modulus $E'$ (mN/m)	Loss modulus $E''$ (mN/m)
295 K, Initial	$5.04 \pm 0.70$	$5.03 \pm 0.68$	$0.41 \pm 0.04$
320 K	$3.98 \pm 0.40$	$3.97 \pm 0.40$	$0.21 \pm 0.02$
295 K, Back	$4.98 \pm 0.52$	$4.97 \pm 0.50$	$0.41 \pm 0.04$

**Table 1.** Moduli of the single droplet, starting at 295 K, at three conditions: initial 295 K, 320 K and back 295 K.

The second single droplet was initially created at 320 K (microgel concentration was still  $5 \times 10^{-3}$  g/mL), equilibrated for two hours to let microgels adsorb onto the heptane-water interface and to reach the thermal equilibrium. Afterwards, it was successively cooled to 295 K, equilibrated for one hour to reach the thermal equilibrium, and then heated back to 320 K, the starting temperature, as shown in Fig. S13. Fig. 13 shows the change of  $\gamma$  as a function of temperature. First, with this single droplet method  $\gamma$  shows a minimum value ( $\sim 13$  mN/m) around 303 K at the cooling process. Upon cooling, microgels swell, and some microgels might be squeezed out of the heptane-water interface. Hence, the interfacial tension decreases and forms the minimum. Second, after these cooling and heating processes,  $\gamma$  does not return to the initial value, for interfacial tensions at initial and back 320 K. The difference between the initial and final values is  $\sim 5$  mN/m. This difference further supports that different ways of preparing the droplets affect the interfacial tensions. Third, in the heating process, similar to the heating process in Fig. 11, no interfacial tension minimum can be observed. Table 2 summarizes the moduli of this single droplet at three conditions: initial 320 K, 295 K, and back 320 K. With this single droplet method, starting at 320 K, the elastic modulus  $E$  is  $\sim 4.58$  mN/m at 295 K. This value is close to the value ( $\sim 5$  mN/m) obtained from fresh droplet method, as shown in Fig. 9 and Table 1. Significant difference ( $\Delta E = E_{Initial,320K} - E_{back,320K} \sim 10$  mN/m) can be observed for the elastic moduli between initial 320 K and back 320 K. This difference further reconfirms that different ways of preparing the droplets affect the microgels laden heptane-water interfacial properties.

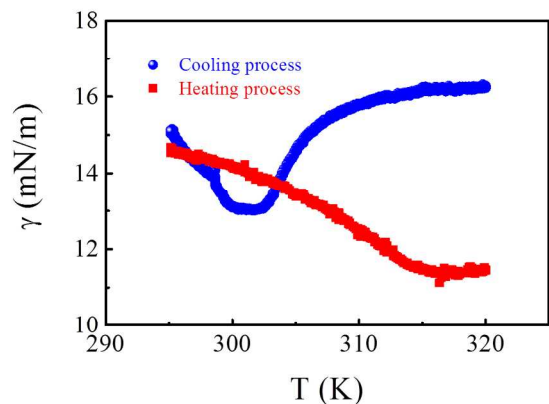


**Fig. 13.** The dynamic interfacial tension  $\gamma_t$  of single droplet, starting at 320 K, in the presence of PNIPAM microgels at various temperatures.

	Complex Modulus $E^*$ (mN/m)	Elastic modulus $E'$ (mN/m)	Loss modulus $E''$ (mN/m)
320 K, Initial	$13.17 \pm 1.32$	$13.09 \pm 1.31$	$1.64 \pm 0.16$
295 K	$4.58 \pm 0.46$	$4.56 \pm 0.46$	$0.38 \pm 0.04$
320 K, Back	$3.71 \pm 0.37$	$3.70 \pm 0.37$	$0.25 \pm 0.03$

**Table 2.** Moduli of the single droplet, starting at 320 K, at three conditions: initial 320 K, 295 K and back 320 K.

From the single droplet experiments (Figs. 12 and 13, Tables 1 and 2), it is evident that different ways of preparing the droplets affect the microgels laden heptane-water interfacial properties. This signifies that there is an irreversible transition among these three states, as shown in Fig. 11. Single droplet experiment, starting at 320 K, shows that state C can go to states B and A in the cooling process.<sup>17</sup> Conversely, from both single droplet experiments, state A can only reach state B but not state C in the heating processes. State B can return to state A in the cooling process but not to state C in the heating process. The irreversible step is that state B cannot approach to state C in the heating process with PNIPAM microgels laden at the heptane-water interface.

### Conclusions

In summary, we investigated the heptane-water interface in the presence of sufficient PNIPAM microgels as a function of temperature. In fresh droplet experiments, we observed  $\gamma_t$  minima around PNIPAM microgel VPTT regardless of microgel aggregates. Both dynamic and static parameters contributed to the formed  $\gamma_t$  minima around VPTT. PNIPAM microgels' deformability dynamically dominated the microgels spreading at the heptane-water interface, while PNIPAM microgels packing and interactions determined the final static equilibrium states. In dilatational rheology measurements at the meso-equilibrium regimes, we found that varied elastic modulus corresponding to the same surface pressure. Based on these results, we proposed PNIPAM microgels would approach to three distinctive states at the heptane-water interface at temperatures below, around, and above VPTT. The single droplet experiments further demonstrated that there existed an irreversible transition among these three states. The revealed results in this paper deepen our understanding of soft, porous, and deformable microgels' behaviors at the oil-water interface, and have important implications for engineering microgels as stimuli-responsive emulsion stabilizers in applications, such as biocatalysis.<sup>6</sup>

## Acknowledgement

The financial support of this work by the Hong Kong Special Administration Region (HKSAR) General Research Fund (CUHK402712, 2130304) and National Natural Science Foundation of China (B040606, 21374091) is gratefully acknowledged. Walter Richtering acknowledges support by the Deutsche Forschungsgemeinschaft, partly within the SFB 985 “Functional microgels and microgel systems”.

## References

1. Y. X. Liu, P. G. Jessop, M. Cunningham, C. A. Eckert and C. L. Liotta, *Science*, 2006, **313**, 958-960.
2. B. Brugger and W. Richtering, *Advanced Materials*, 2007, **19**, 2973-2978.
3. B. Brugger, B. A. Rosen and W. Richtering, *Langmuir*, 2008, **24**, 12202-12208.
4. B. Brugger, S. Ruetten, K.-H. Phan, M. Moeller and W. Richtering, *Angewandte Chemie-International Edition*, 2009, **48**, 3978-3981.
5. B. Brugger, J. Vermant and W. Richtering, *Physical Chemistry Chemical Physics*, 2010, **12**, 14573-14578.
6. S. Wiese, A. C. Spiess and W. Richtering, *Angewandte Chemie-International Edition*, 2013, **52**, 576-579.
7. R. Pelton, *Advances in Colloid and Interface Science*, 2000, **85**, 1-33.
8. M. Das, H. Zhang and E. Kumacheva, in *Annual Review of Materials Research*, 2006, vol. 36, pp. 117-142.
9. A. Fernandez-Nieves, H. Wyss, J. Mattsson and D. A. Weitz, *Microgel Suspensions*, Wiley, Singapore, 2011.
10. L. A. Lyon and A. Fernandez-Nieves, *Annual Review of Physical Chemistry*, 2012, **63**, 25-43.
11. H. G. Schild, *Progress in Polymer Science*, 1992, **17**, 163-249.
12. T. Ngai, H. Auweter and S. H. Behrens, *Macromolecules*, 2006, **39**, 8171-8177.
13. T. Ngai, S. H. Behrens and H. Auweter, *Chemical Communications*, 2005, 331-333.
14. B. Brugger and W. Richtering, *Langmuir*, 2008, **24**, 7769-7777.
15. M. Destribats, M. Eyharts, V. Lapeyre, E. Sellier, I. Varga, V. Ravaine and V. Schmitt, *Langmuir*, 2014, **30**, 1768-1777.
16. M. Destribats, B. Faure, M. Birot, O. Babot, V. Schmitt and R. Backov, *Advanced Functional Materials*, 2012, **22**, 2642-2654.
17. M. Destribats, V. Lapeyre, E. Sellier, F. Lea-Calderon, V. Ravaine and V. Schmitt, *Langmuir*,

- 2012, **28**, 3744-3755.
18. M. Destribats, V. Lapeyre, E. Sellier, F. Leal-Calderon, V. Schmitt and V. Ravaine, *Langmuir*, 2011, **27**, 14096-14107.
  19. M. Destribats, V. Lapeyre, M. Wolfs, E. Sellier, F. Leal-Calderon, V. Ravaine and V. Schmitt, *Soft Matter*, 2011, **7**, 7689-7698.
  20. M. Destribats, M. Wolfs, F. Pinaud, V. Lapeyre, E. Sellier, V. Schmitt and V. Ravaine, *Langmuir*, 2013, **29**, 12367-12374.
  21. Z. Li, K. Geisel, W. Richtering and T. Ngai, *Soft Matter*, 2013, **9**, 9939-9946.
  22. Z. Li, T. Ming, J. Wang and T. Ngai, *Angewandte Chemie-International Edition*, 2009, **48**, 8490-8493.
  23. Z. Li and T. Ngai, *Langmuir*, 2010, **26**, 5088-5092.
  24. Z. Li and T. Ngai, *Colloid and Polymer Science*, 2011, **289**, 489-496.
  25. Z. Li, X. Wei, T. Ming, J. Wang and T. Ngai, *Chemical Communications*, 2010, **46**, 8767-8769.
  26. Z. Li, X. Wei and T. Ngai, *Chemical Communications*, 2011, **47**, 331-333.
  27. S. Schmidt, T. Liu, S. Ruetten, K.-H. Phan, M. Moeller and W. Richtering, *Langmuir*, 2011, **27**, 9801-9806.
  28. T. Liu, S. Seiffert, J. Thiele, A. R. Abate, D. A. Weitz and W. Richtering, *Proceedings of the National Academy of Sciences of the United States of America*, 2012, **109**, 384-389.
  29. S. Tsuji and H. Kawaguchi, *Langmuir*, 2008, **24**, 3300-3305.
  30. K. Geisel, L. Isa and W. Richtering, *Langmuir*, 2012, **28**, 15770-15776.
  31. Z. Li and T. Ngai, *Nanoscale*, 2013, **5**, 1399-1410.
  32. W. Richtering, *Langmuir*, 2012, **28**, 17218-17229.
  33. V. Schmitt and V. Ravaine, *Current Opinion in Colloid & Interface Science*, 2013, **18**, 532-541.
  34. K. Geisel, L. Isa and W. Richtering, *Angewandte Chemie International Edition*, 2014, **126**, 5005-5009.
  35. C. Monteux, C. Marliere, P. Paris, N. Pantoustier, N. Sanson and P. Perrin, *Langmuir*, 2010, **26**, 13839-13846.
  36. J. Zhang and R. Pelton, *Langmuir*, 1996, **12**, 2611-2612.
  37. J. Zhang and R. Pelton, *Colloids and Surfaces a-Physicochemical and Engineering Aspects*, 1999, **156**, 111-122.
  38. J. Zhang and R. Pelton, *Journal of Polymer Science Part A: Polymer Chemistry*, 1999, **37**, 2137-2143.
  39. J. Zhang and R. Pelton, *Langmuir*, 1999, **15**, 8032-8036.
  40. B. J. Berne and R. Pecora, *Dynamic Light Scattering: With Applications to Chemistry, Biology,*

- and Physics*, Dover Publications, New York, 2000.
41. H. Ohshima, *Colloid Polym Sci*, 2007, **285**, 1411-1421.
  42. Y. Rotenberg, L. Boruvka and A. W. Neumann, *Journal of Colloid and Interface Science*, 1983, **93**, 169-183.
  43. X. Y. Hua and M. J. Rosen, *Journal of Colloid and Interface Science*, 1988, **124**, 652-659.
  44. R. Miller and G. Kretzschmar, *Advances in Colloid and Interface Science*, 1991, **37**, 97-121.
  45. M. Hoorfar and A. W. Neumann, *Advances in Colloid and Interface Science*, 2006, **121**, 25-49.
  46. A. W. Adamson and A. P. Gast, *Physical Chemistry of Surfaces*, 6th edn., Wiley-Interscience, Canada, 1997.
  47. S. S. Dukhin, G. Kretzschmar and R. Miller, *Dynamics of Adsorption at Liquid Interfaces*, Elsevier, The Netherlands, 1995.
  48. J. Eastoe and J. S. Dalton, *Advances in Colloid and Interface Science*, 2000, **85**, 103-144.
  49. L. Isa, E. Amstad, K. Schwenke, E. Del Gado, P. Ilg, M. Kroger and E. Reimhult, *Soft Matter*, 2011, **7**, 7663-7675.
  50. J. T. Russell, Y. Lin, A. Boker, L. Su, P. Carl, H. Zettl, J. B. He, K. Sill, R. Tangirala, T. Emrick, K. Littrell, P. Thiyagarajan, D. Cookson, A. Fery, Q. Wang and T. P. Russell, *Angewandte Chemie-International Edition*, 2005, **44**, 2420-2426.
  51. N. Glaser, D. J. Adams, A. Böker and G. Krausch, *Langmuir*, 2006, **22**, 5227-5229.
  52. S. Kutuzov, J. He, R. Tangirala, T. Emrick, T. P. Russell and A. Boker, *Physical Chemistry Chemical Physics*, 2007, **9**, 6351-6358.
  53. K. Du, E. Glogowski, T. Emrick, T. P. Russell and A. D. Dinsmore, *Langmuir*, 2010, **26**, 12518-12522.
  54. X. Wu, R. H. Pelton, A. E. Hamielec, D. R. Woods and W. McPhee, *Colloid and Polymer Science*, 1994, **272**, 467-477.
  55. M. Stieger, W. Richtering, J. S. Pedersen and P. Lindner, *Journal of Chemical Physics*, 2004, **120**, 6197-6206.
  56. E. Daly and B. R. Saunders, *Physical Chemistry Chemical Physics*, 2000, **2**, 3187-3193.
  57. B. R. Saunders and B. Vincent, *Advances in Colloid and Interface Science*, 1999, **80**, 1-25.
  58. A. F. Routh and B. Vincent, *Langmuir*, 2002, **18**, 5366-5369.
  59. T. A. Vilgis and M. Stapper, *European Physical Journal B*, 1998, **2**, 69-74.
  60. Y. Cohin, M. Fisson, K. Jourde, G. G. Fuller, N. Sanson, L. Talini and C. Monteux, *Rheologica Acta*, 2013, **52**, 445-454.
  61. S. M. Hashmi and E. R. Dufresne, *Soft Matter*, 2009, **5**, 3682-3688.
  62. B. Sierra-Martin, Y. Laporte, A. B. South, L. A. Lyon and A. Fernandez-Nieves, *Physical Review*

- E*, 2011, **84**, 011406.
63. P. Voudouris, D. Florea, P. van der Schoot and H. M. Wyss, *Soft Matter*, 2013, **9**, 7158-7166.
  64. S. Hirotsu, *Macromolecules*, 1990, **23**, 903-905.
  65. D. M. Heyes and A. C. Branka, *Soft Matter*, 2009, **5**, 2681-2685.
  66. F. Scheffold, P. Diaz-Leyva, M. Reufer, N. Ben Braham, I. Lynch and J. L. Harden, *Physical Review Letters*, 2010, **104**, 128304.
  67. W. Song, Y. Guan, Y. Zhang and X. X. Zhu, *Soft Matter*, 2013, **9**, 2629-2636.
  68. P. Holmqvist, P. S. Mohanty, G. Naegele, P. Schurtenberger and M. Heinen, *Physical Review Letters*, 2012, **109**, 048302.
  69. S. C. Russev, N. Alexandrov, K. G. Marinova, K. D. Danov, N. D. Denkov, L. Lyutov, V. Vulchev and C. Bilke-Krause, *Rev. Sci. Instrum.*, 2008, **79**, 104102.
  70. J. Benjamins, A. Cagna and E. H. LucassenReynders, *Colloids and Surfaces a-Physicochemical and Engineering Aspects*, 1996, **114**, 245-254.